Environ. Sci. Technol. **2006**, *40,* 1511−1515

Physical Structures of Lipid Layers on Pyrite

XIANG V. ZHANG,[†] TREAVOR A. KENDALL,[†] JUN HAO,[‡] DANIEL R. STRONGIN,[‡,∥] MARTIN A. A. SCHOONEN,[§,∥] AND SCOT T. MARTIN*,[†]

Division of Engineering and Applied Sciences, Harvard University, Cambridge, Massachusetts 02138, Department of Chemistry, Temple University, Philadelphia, Pennsylvania 19122, Geosciences Department and Center for Environmental Molecular Science, The State University of New York at Stony Brook, Stony Brook, New York 11794

The physical structures of lipid layers on pyrite (FeS_2), a ubiquitous sulfide mineral, were studied in air and in water by atomic force microscopy (AFM). Egg PC, a phospholipid that forms bilayer structures on atomically flat substrates, was investigated, and our experimental observations show that this lipid formed bilayers on an atomically rough pyrite surface, as inferred by a measured layer thickness of 5.0 ± 0.2 nm. The surface coverage of the lipid coating increased from approximately 15% to 80% when the concentration of the lipid suspension was increased from 0.014 to 0.15 mM. Although further increases up to 1.5 mM resulted in an incremental increase in surface coverage of only 5%, multilayer structures of 20- to 40-nm height formed on top of the first bilayer. The findings provide a structural explanation for the results of earlier kinetic studies showing that the presence of the lipid decreases the rate of pyrite oxidation in air and in water. Lipid coatings applied to iron-sulfide bearing minerals are a possible approach to preventing oxidation and acidification and thereby mitigating environmental damage that can result from acid mine drainage.

1. Introduction

Organic layers on mineral surfaces may substantially alter mineral reactivity (*1*). Predictions of the effects of these layers on surface reactivity will be improved by a better understanding of the structure of these layers. Lipids are one class of biogenic organic material capable of forming structured layers. Atomic force microscopy was previously used to characterize lipid structures on gold, mica, and glass (*2*−*7*). The results for those surfaces indicate that there are several common aspects of the physical structures of lipid layers on surfaces (*8*). Unruptured lipid vesicles can deposit on surfaces exposed to low concentrations of lipid suspensions (*6*). Lipid vesicles can rupture and fuse on surfaces to form individual lipid bilayer patches (*6*, *9*). Lipid bilayer patches can merge to form larger ones, eventually covering the entire surface (*5*). Lipid monolayers, bilayers, and vesicles can adsorb to stratum bilayer structures formed on the surface, thus leading to multilayer lipid structures (*5*, *10*). Unknown at the outset of this study, however, were the similarities and the differences between these common structures of lipid layers on gold, mica, glass and other atomically flat surfaces and the physical structures of lipid layers on natural pyrite and other minerals having rough and defect-laden surfaces. The current study addresses whether a natural pyrite surface is able to support an adsorbed lipid bilayer structure.

In previous work on pyrite, the physical structures of lipid layers were inferred indirectly from infrared spectra (*11*). The results indicated that the polar headgroups of the lipids were bound to the surface of pyrite. The consequent hypotheses were that close-packed lipid bilayers form and that they act as a barrier to oxidation by preventing water access to the pyrite surface. Unanswered questions included the following: (*i*) What types of structural motifs do the lipids adopt on the pyrite surface? (*ii*) How do the structures and coverages of the lipids on the pyrite depend on the lipid concentration in suspension? To address these questions, we employ atomic force microscopy in the present study to directly observe the physical structures of the lipid layers and their surface coverages on pyrite.

The lipid used in the current study is L-α-phosphatidylcholine, hydrogenated (egg, chicken) lipid (abbreviated Egg PC). The chemical structure of Egg PC is as follows (*12*):

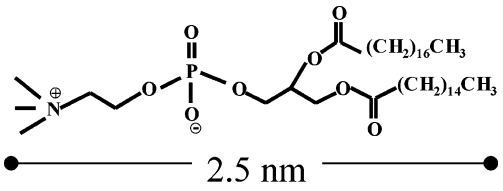

Our reasons for choosing this specific lipid are two-fold. First, Egg PC is effective in suppressing pyrite oxidation in air and in water (*11*, *13*). Second, Egg PC has been used previously as a model system to study lipid−mineral interactions (*5*, *6*, *11*, *14*).

2. Experimental Section

A stock suspension of lipid was prepared by adding Egg PC solid (Avanti Polar Lipids, Alabaster, AL) to 100 mM NaCl at 298 K and pH 7. The suspension was vortexed for 20 min and sonicated for 45 min at room temperature. The sonication homogenized the lipid suspension by disrupting large multilamellar vesicles to form small unilamellar vesicles (*6*). A portion of the stock suspension, referred to hereafter as "high concentration" (viz. 1.5 mM or 1.14 g/L), was diluted with buffer solution to make a "medium concentration" suspension of 0.15 mM. A "low concentration" suspension was prepared by centrifuging a portion of the high concentration suspension at 16 000*g* and 10 °C for 35 min and extracting the supernatant (*6*). The centrifuging removed large vesicles, leaving in the supernatant only vesicles smaller than 100 nm. The lipid concentration in the supernatant, determined by total organic carbon analysis (Shimadzu TOC-Vws), was 0.014 mM. The above procedures thus resulted in low (0.014 mM), medium (0.15 mM), and high (1.5 mM) concentrations of lipid in 100 mM NaCl at pH 7.

Single-crystal pyrite cubes (Navajun, Spain), purchased from Ward's Natural Science (Rochester, NY), were cut using

* Corresponding author e-mail: scot_martin@harvard.edu. www.deas.harvard.edu/environmental-chemistry.
[†] Harvard University.
[‡] Temple University.
[§] Geosciences Department, The State University of New York at Stony Brook.
[∥] Center for Environmental Molecular Science, The State University of New York at Stony Brook.

10.1021/es051794q CCC: $33.50
Published on Web 01/24/2006

a diamond trim-saw to 12.8 × 12.8 × 1.00 mm^3. Uncut (100) growth faces remained on one side of each sample to serve as the experimental surfaces. The pyrite samples were cleaned by sequential 15-min exposures to chloroform, acetone, and methanol in an ultrasonic bath at room temperature. The samples were rinsed with deoxygenated ultrapure water (18 MΩ-cm) and etched in HCl solution at pH 2 for 1 min to remove oxidized material from the surface (*15*). After etching, the samples were rinsed again with deoxygenated water and dried with a stream of ultrapure argon gas.

For a single experiment, lipid was deposited on the (100) surface of a pyrite sample by exposing the mineral to one of the deoxygenated low, medium, or high concentration suspensions for 20 min in a beaker. One of the two following protocols was subsequently followed: (*i*) If a sample was to be imaged in air, it was rinsed in deoxygenated water for 15 s to remove NaCl and any loosely bonded lipid and then dried in a stream of argon. (*ii*) If a sample was to be imaged under aqueous conditions, it was rinsed and then placed in a 100 mM deoxygenated NaCl buffer solution.

Micrographs of the lipid-coated sample were collected with a Nanoscope IIIa MultiMode AFM (Veeco, Inc., Santa Barbara, CA). Tapping-mode images in air were collected using Si_3N_4 probes having a nominal force constant of 39 N m^{-1} and a resonant frequency of 288 kHz (Olympus, MicroCantilever, Japan). Tapping-mode images in liquid were collected using Si_3N_4 probes having a nominal force constant of 0.38 N m^{-1} and a resonant frequency of 30 kHz in the liquid. The AFM images were processed off-line using WSxM software (Nanotec Electronica, Madrid, Spain).

For images collected under aqueous conditions, a 100 μL droplet of 100 mM deoxygenated NaCl buffer solution was injected into a liquid cell secured above the sample. The droplet completely enveloped the cantilever and the imaged portion of the surface.

To determine the position of pyrite surface once coated by a lipid film, in selected experiments we employed scraping (*5*, *10*, *16*). In this procedure, the surface was scanned with the AFM tip at a high contact force ranging from 600 to 2000 nN normal to the surface and at a tip velocity of 3.5 μm s^{-1}. The scrape force was controlled by monitoring force−distance curves and adjusting the setpoint accordingly. Under the high force, the lipid layer was displaced, and the thickness of the lipid layer could therefore be determined by measuring the height difference between the scraped and unscraped areas in a follow-on tapping-mode AFM image (*5*, *10*, *16*).

3. Results and Discussion

3.1 Lipid Layer on Pyrite Surface in Air. The pyrite surface viewed under an optical microscope had terraces every 10 to 20 μm. The imaging with AFM was carried out on the optically flat terraces. Figure 1 shows an AFM micrograph of the cleaned pyrite terrace before lipid deposition. Our study targeted areas of the terrace having few etch pits and a surface roughness of less than 1 nm (see upper left portion of Figure 1). Even so, this surface had a greater roughness than the nearly atomically flat surfaces (roughness under 0.2 nm) employed in previous studies of supported lipid bilayers (*2*−*7*).

3.1.1 Low Concentration (0.014 mM). Given the roughness of the pyrite surface, we were not certain prior to conducting the experiments that a lipid bilayer would form. An analysis of the micrographs, however, implies that the Egg PC forms a bilayer on the pyrite surface. Figure 2a and b show lipid islands having 50- to 100-nm lateral dimensions and 5-nm heights (Figure 2c). The observed lateral dimensions are in agreement with the reported dimensions of individual vesicles in the supernatant of the centrifuged preparation (*6*). The surfaces of the lipid islands are flat across a 100-nm width, having a measured height variance of less than 0.5 nm. The

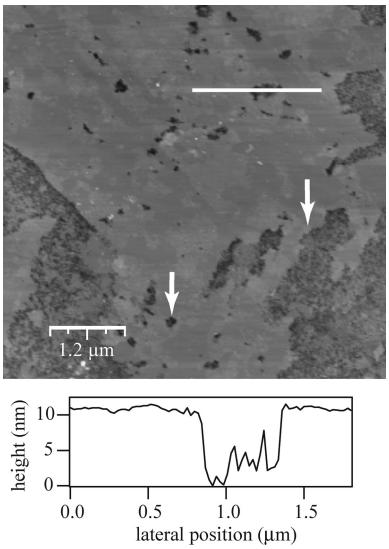

FIGURE 1. Micrograph of an optically flat terrace on the pyrite surface. Roughness occurs, however, at the nanometer scale. Arrows point to areas etched by acid rinsing at pH 2. The white line indicates the location of the height cross section shown below the micrograph. (Scan size is 6.0 × 6.0 μm^2. Micrograph is recorded in air as height data in tapping mode.)

average of height measurements of twenty islands is 5.1 nm with a two-standard-error uncertainty of 0.2 nm (95% confidence limits). Egg PC layers of thickness from 4.0 to 5.5 nm are presumed to imply a bilayer structure (*5*−*7*, *9*). This thickness range accounts for variability in factors such as salt concentration, measurement error, or image force.

An important control experiment was to verify the exact position of the pyrite−lipid interface and thus the coating thickness. To accomplish this, we employed contact-mode scraping to remove the lipid coating and expose the pyrite surface (*5*, *10*, *16*). Scraping resulted in the displacement of lipid islands into piles at the edges of the scan area transversed by the AFM tip. No height difference between the scraped and the unscraped bare pyrite areas was observed (data not shown). Therefore, the islands shown in Figure 2 resided directly on the pyrite surface and not on top of another lipid layer. Using this experimental observation to set the threshold height parameter in a particle analysis algorithm, we find that the lipid islands shown in Figure 2a covered 15−20% of the total pyrite surface. An implication could be that such a limited coverage is insufficient to significantly reduce the rate of pyrite oxidation in air.

3.1.2 Medium Concentration (0.15 mM). As an experimental test to determine whether we could increase the surface lipid coverage, pyrite was exposed to a higher concentration of lipid suspension. Interconnected lipid patches formed with a coverage of 80−90% of the surface. In most areas of the surface, a bilayer formed (Figure 3a). Scraping the surface with the AFM tip resulted in the recessed square area shown in Figure 4. The average height difference inside and outside of the scraped area was 5.1 ± 0.3 nm, indicating that the lipid bilayer patches directly overlay the pyrite surface. The average and its two-standard-error uncertainty were based on 12 observations. In other areas of the surface, thicker sequences of lipid formed on top of the bilayer with heights ranging from 10 to 20 nm (Figure 3b). These thick layers were likely due to the rupture of lipid vesicles on top of existing bilayer patches, thus resulting in multilayer structures (*5*). Figure 3b shows the staircase pattern of the multilayer structures. The height of each step was 2.5 nm, corresponding to a monolayer of lipid. The lipid coverage was between 80 and 90%, of which 20 to 30% was composed

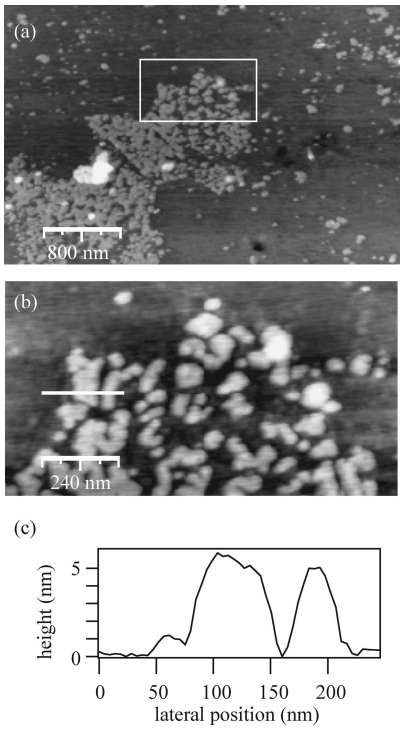

FIGURE 2. (a) Micrograph showing lipid islands on the pyrite surface after exposure to the low concentration lipid suspension (0.014 mM). Height images (4.0 × 2.6 μm^2) are collected in air using tapping mode. (b) Expanded view of the boxed region in *a* (1.2 × 0.7 μm^2). (c) Cross section of line shown in *b*.

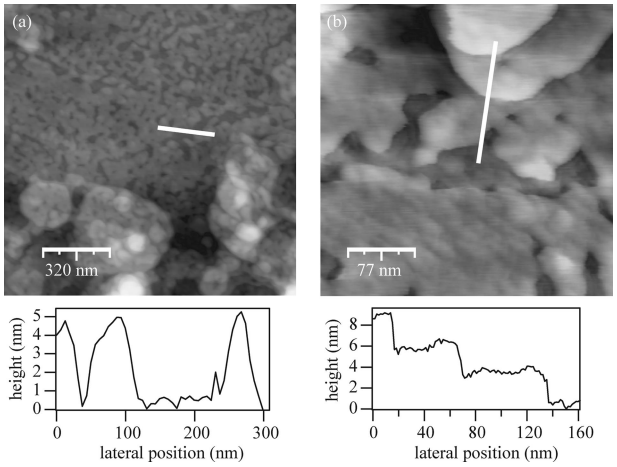

FIGURE 3. Micrographs of the pyrite surface after exposure to the medium concentration (0.15 mM) lipid suspension. Height images are collected in air using tapping mode. (a) Partial coverage by a 5-nm lipid bilayer is apparent in the upper portion of this image (1.6 × 1.6 μm^2 scan). (b) Multilayer lipid structure occurs elsewhere on the surface. The 2.5-nm steps in the cross section correspond to a lipid monolayer. Scan size is 390 × 390 nm^2.

of the thicker multilayer structure. We hypothesize that this lipid structure could significantly slow air oxidation of pyrite.

3.1.3 High Concentration (1.5 mM). Previous pyrite oxidation experiments showed that at high lipid concentration (1.5 mM) the air oxidation rate of the mineral was significantly reduced compared to the absence of lipid (see Figure 6 of ref *11*). Increasing the lipid concentration by a further order of magnitude relative to the medium lipid concentration led to a small increase in total surface coverage (to 92%) but a large increase in the coverage by multilayer structures and an increase in their heights (Figure 5). The cross sections show that there was an underlying bilayer

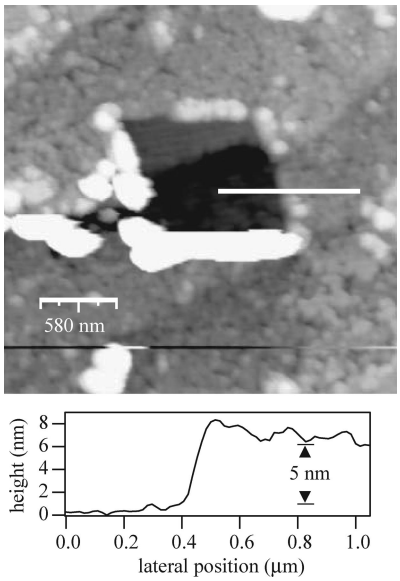

FIGURE 4. Micrograph and cross section after scraping a surface previously treated by the medium concentration (0.15 mM) lipid suspension. The cross section shows that the lipid layer is 5-nm thick. The height image (2.9 × 2.9 μm^2) is collected in air using tapping mode after scraping in contact mode. The scrape field of 1.0 × 1.0 μm^2 is apparent.

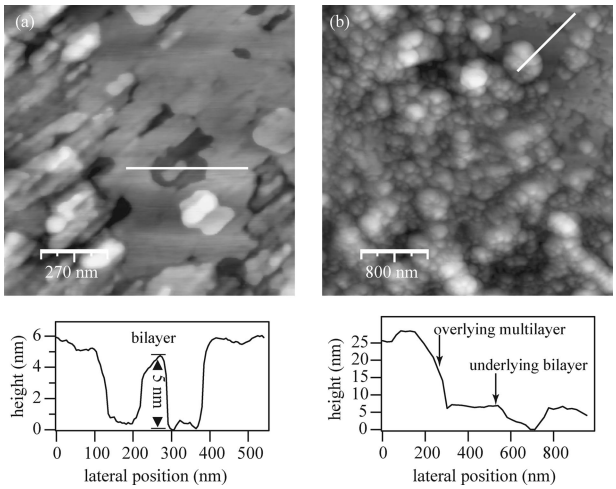

FIGURE 5. Micrographs of the pyrite surface after exposure to the high concentration (1.5 mM) lipid suspension. Height images are collected in air using tapping mode. (a) Cross section shows that the base stratum is a lipid bilayer of 5-nm thickness (1.3 × 1.3 μm^2 scan). (b) Cross section shows that multilayer structures of 20- to 40-nm height form on the bilayer stratum (4.0 × 4.0 μm^2 scan). The pyrite surface is located at $z = 0$ nm in both cross sections.

having a thickness of 5 nm. On top of the bilayer, lipid multilayers of 20- to 40-nm thickness as well as unruptured vesicles were observed (Figure 5b). The surface coverage was 92% of the total pyrite surface; 80% of the surface was covered with lipid multilayers. Kumar and Hoh have previously reported the formation of multilayer lipid structures on mica at high lipid concentrations (*10*). The increased lipid coverage between medium and high concentrations could further decrease the air oxidation rate of pyrite; however, the largest marginal gain may be found in the low to medium jump, under the assumption that rate correlates with surface coverage rather than layer thickness.

3.2 Lipid Layer on Pyrite Surface in Aqueous Solution. Under aqueous conditions, the lipid coating formed bilayer structures similar to those observed when imaging in air. Figure 6 shows an example of the results under aqueous

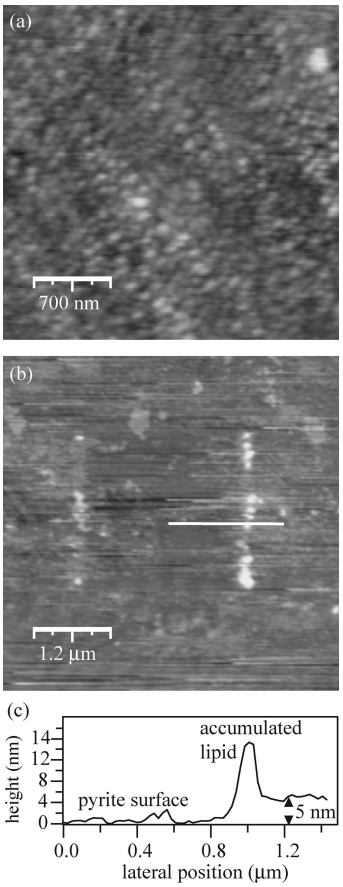

FIGURE 6. Micrographs of the pyrite surface after exposure to the medium concentration (0.15 mM) lipid suspension. The liquid cell of the AFM is employed to collect tapping-mode height images in 100 mM NaCl and pH 7. (a) Pyrite surface is covered by lipid patches. Scan size is 3.0 × 3.0 μm^2. (b) Micrograph (5.1 × 5.1 μm^2) and (c) cross section after scraping (1.5 × 1.5 μm^2 scrape field) a surface in the presence of the medium concentration lipid suspension. The cross section across the edge of the scrape field shows accumulated lipid at the edge and a lipid layer thickness of 5 nm.

conditions. After exposure of the pyrite surface to a medium concentration lipid suspension (0.15 mM), 100-nm patches of lipid were observed when imaged in 100 mM NaCl buffer solution (Figure 6a). Scraping the coating using the AFM tip showed that the thickness of the lipid layer was 4.8 ± 0.3 nm (Figure 6b and c; 21 observations), again suggesting a bilayer structure. The lipid surface coverage was 90%. The similarities in results between air and aqueous conditions may be rationalized by the hydrophobic chain−chain interactions that drive the structuring under both humid air and aqueous conditions. Previous oxidation experiments at high concentration and pH of 1 and 2 showed that the aqueous oxidation rate was reduced by 70% compared to that in the absence of the lipid (see Figure 7 of ref *11*).

Cremer and Boxer suggested that a 1-nm layer of water between mica and a lipid bilayer conferred mobility to the bilayer (*7*, *14*). We tested this possibility for the lipid bilayers on pyrite by employing indentation experiments (*5*, *10*, *16*). Although there was flexibility in the lipid layer, we did not observe any movement of the lipid layer (data not shown). We therefore have no experimental evidence consistent with an intermediate water layer between the lipid layer and pyrite surface. This conclusion is reinforced by the inner-sphere interactions between the phosphate group and the pyrite surface that were concluded from the infrared observations presented in ref *11*.

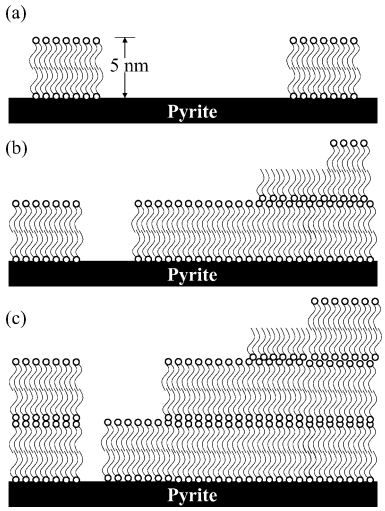

FIGURE 7. Depiction of bilayer and multilayer lipid structures on the pyrite surface for increasing lipid concentration: (a) low, (b) medium, and (c) high concentrations.

4. Implications

Prior to this study, the physical structures of lipid layers on a pyrite surface had not been directly observed. AFM imaging of the pyrite surface in air or in solution after the mineral was exposed to Egg PC concentrations ranging from 0.14 to 1.5 mM showed the presence of lipid bilayers and multilayers. Figure 7 shows a diagram that summarizes our experimental observations. Prior literature reports have shown that surface features such as defects or steps acted as a barrier for lipid bilayer formation and growth (*7*, *17*). These reports therefore suggested that bilayer structures may not form on natural mineral surfaces because of their roughness. On the contrary, our results indicate, for the first time, that a uniform bilayer structure can form on a mineral surface that is less than atomically flat. Although we investigated only Egg PC, other phosphocholine lipids that form bilayer structures in solution can be reasonably supposed to also form a supported bilayer structure on pyrite.

The protection by adsorbed lipid layers of metal sulfides in the environment has been proposed by us (*11*, *13*, *18*) as a potential solution to avoiding the oxidation of pyrite-containing mine waste that leads to acidic water outflow, often called acid mine drainage (*19*−*22*). The outflow can endanger ecosystems and can threaten water supplies. As a result, both cleanup approaches and pollution-prevention strategies are being considered and applied in some cases. One cleanup method is to employ alkaline reagents such as calcite, sodium carbonate, or aqueous NaOH in affected areas. A drawback of this method, however, is the need to apply excess material, which often leads to caustic water runoff. Moreover, the alkaline reagent must be reapplied on a frequent basis. As an alternative approach, some researched pollution-prevention strategies have included encapsulation of pyrite grains with silica coatings (*23*, *24*) and complexation of catalytic oxidation centers (mainly surficial Fe^{3+} defects) with humic acid or other organic ligands (*25*, *26*). These strategies, however, have been unsuccessful under the low pH and highly oxic chemical environments of acid mine drainage (*27*, *28*). As a different approach suitable to the conditions of acid mine drainage, we proposed and demonstrated the use of two-tail lipid coatings to inhibit pyrite oxidation at low pH (*11*, *13*, *18*).

The results of the current study reveal the structure of lipid layers on the pyrite surface and therefore help to develop a mechanistic understanding of the oxidation suppression process. Our AFM results support previous findings that the

lipid forms a hydrophobic barrier to isolate the pyrite surface from water and ionic constituents such as aqueous Fe^{3+} ions (*19*, *29*). Although nonpolar O_2 diffuses readily through lipid membranes, pyrite oxidation in the absence of water is slow (*30*). Moreover, although the imaging work in this paper was carried out at pH 7 whereas acid mine drainage conditions are often pH 1−2, our previous infrared results suggest that the lipid bilayer of Egg PC on pyrite is not strongly affected by pH (cf. Figure 9 of ref *11*), perhaps because the lipid bilayer yields a hydrophobic environment having little sensitivity to aqueous conditions. We conclude that the mechanism of action of Egg PC is the formation of a physical bilayer barrier that inhibits the approach to the pyrite surface of water and other catalytic dissolved ionic constituents such as aqueous Fe^{3+}.

Acknowledgments

This study was supported by the Chemical Sciences, Geosciences, and Biosciences Division of the Office of Basic Energy Sciences in the U.S. Department of Energy by separate awards to S.T.M., D.R.S., and M.A.S. This research was also partially supported by the Center for Environmental Molecular Science (CEMS) at Stony Brook (NSF-CHE-0221934).

Literature Cited

(1) Templeton, A. S.; Trainor, T. P.; Traina, S. J.; Spormann, A. M.; Brown, G. E. Pb(II) distributions at biofilm-metal oxide interfaces. *Proc. Natl. Acad. Sci. U. S. A.* **2001**, *98*, 11897−11902.
(2) Dufrene, Y. F.; Lee, G. U. Advances in the characterization of supported lipid films with the atomic force microscope. *Biochim. Biophys. Acta* **2000**, *1509*, 14−41.
(3) Schneider, J.; Dufrene, Y. F.; Barger, W. R. J.; Lee, G. U. Atomic force microscope image contrast mechanisms on supported lipid bilayers. *Biophys. J.* **2000**, *79*, 1107−1118.
(4) Stephens, S. M.; Dluhy, R. A. In-situ and ex-situ structrural analysis of phospholipid-supported planar bilayers using infrared spectroscopy and atomic force microscopy. *Thin Solid Films* **1996**, *284−285*, 381−386.
(5) Egawa, H.; Furusawa, K. Liposome adhesion on mica surface studied by atomic force microscopy. *Langmuir* **1999**, *15*, 1660−1666.
(6) Liang, X. M.; Mao, G. Z.; Ng, K. Y. S. Probing small unilamellar EggPC vesicles on mica surface by atomic force microscopy. *Colloids Surf., B* **2004**, *34*, 41−51.
(7) Cremer, P. S.; Boxer, S. G. Formation and spreading of lipid bilayers on planar glass supports. *J. Phys. Chem. B* **1999**, *103*, 2554−2559.
(8) Sackmann, E. Supported membranes: Scientific and practical applications. *Science* **1996**, *271*, 43−48.
(9) Schonherr, H.; Johnson, J. M.; Lenz, P.; Frank, C. W.; Boxer, S. G. Vesicle adsorption and lipid bilayer formation on glass studied by atomic force microscopy. *Langmuir* **2004**, *20*, 11600−11606.
(10) Kumar, S.; Hoh, J. H. Direct visualization of vesicle-bilayer complexes by atomic force microscopy. *Langmuir* **2000**, *16*, 9936−9940.
(11) Zhang, X.; Borda, M. J.; Schoonen, M. A. A.; Strongin, D. R. Adsorption of phospholipids on pyrite and their effect on surface oxidation. *Langmuir* **2003**, *19*, 8787−8792.
(12) Avanti Polar Lipids, Inc, Alabaster, AL. Product data sheet 830059.
(13) Elsetinow, A. R.; Borda, M. J.; Schoonen, M. A. A.; Strongin, D. R. Suppression of pyrite oxidation in acidic aqueous environments using lipids having two hydrophobic tails. *Adv. Environ. Res.* **2003**, *7*, 969−974.
(14) Kim, J.; Kim, G.; Cremer, P. S. Investigations of water structure at the solid/liquid interface in the presence of supported lipid bilayers by vibrational sum frequency spectroscopy. *Langmuir* **2001**, *17*, 7255−7260.
(15) Elsetinow, A. R.; Schoonen, M. A. A.; Strongin, D. R. Aqueous geochemical and surface science investigation of the effect of phosphate on pyrite oxidation. *Environ. Sci. Technol.* **2001**, *35*, 2252−2257.
(16) Mou, J.; Yang, J.; Huang, C.; Shao, Z. Alcohol induces interdigitated domains in unilamellar phosphatidylcholine bilayers. *Biochemistry* **1994**, *33*, 9981−9985.
(17) Groves, J. T.; Ulman, N.; Boxer, S. G. Micropatterning fluid lipid bilayers on solid supports. *Science* **1997**, *275*, 651−653.
(18) Zhang, X.; Borda, M. J.; Schoonen, M. A. A.; Strongin, D. R. Pyrite oxidation inhibition by a cross-linked lipid coating. *Geochem. Trans.* **2003**, *4*, 8−11.
(19) Evangelou, V. P.; Zhang, Y. L. A Review − Pyrite Oxidation Mechanisms and Acid-Mine Drainage Prevention. *Crit. Rev. Environ. Sci. Technol.* **1995**, *25*, 141−199.
(20) Elberling, B.; Nicholson, R. V.; Scharer, J. M. A Combined Kinetic and Diffusion-Model for Pyrite Oxidation in Tailings − a Change in Controls with Time. *J. Hydrol.* **1994**, *157*, 47−60.
(21) Banks, D.; Younger, P. L.; Arnesen, R. T.; Iversen, E. R.; Banks, S. B. Mine-water chemistry: the good, the bad and the ugly. *Environ. Geol.* **1997**, *32*, 157−174.
(22) Edwards, K. J.; Bond, P. L.; Druschel, G. K.; McGuire, M. M.; Hamers, R. J.; Banfield, J. F. Geochemical and biological aspects of sulfide mineral dissolution: lessons from Iron Mountain, California. *Chem. Geol.* **2000**, *169*, 383−397.
(23) Evangelou, V. P. *Pyrite Oxidation and Its Control*; CRC Press: New York, 1995.
(24) Evangelou, V. P. Potential Microencapsulation of Pyrite by Artificial Inducement of Ferric Phosphate Coatings. *J. Environ. Qual.* **1995**, *24*, 535−542.
(25) Peiffer, S.; Stubert, I. The oxidation of pyrite at pH 7 in the presence of reducing and nonreducing Fe(III)-chelators. *Geochim. Cosmochim. Acta* **1999**, *63*, 3171−3182.
(26) Lalvani, S. B.; Zhang, G.; Lalvani, L. S. Coal pyrite passivation due to humic acids and lignin treatment. *Fuel Sci. Technol. Int.* **1996**, *14*, 1291−1313.
(27) Marchand, E. A.; Plumb, P. Minerals and mine drainage. *Water Environ. Res.* **2004**, *76*, 1684−1740.
(28) Nordstrom, D. K.; Alpers, C. N.; Ptacek, C. J.; Blowes, D. W. Negative pH and extremely acidic mine waters from Iron Mountain, California. *Environ. Sci. Technol.* **2000**, *34*, 254−258.
(29) Moses, C. O.; Nordstrom, D. K.; Herman, J. S.; Mills, A. L. Aqueous Pyrite Oxidation by Dissolved-Oxygen and by Ferric Iron. *Geochim. Cosmochim. Acta* **1987**, *51*, 1561−1571.
(30) Guevremont, J. M.; Bebie, J.; Elsetinow, A. R.; Strongin, D. R.; Schoonen, M. A. A. Reactivity of the (100) plane of pyrite in oxidizing gaseous and aqueous environments: Effects of surface imperfections. *Environ. Sci. Technol.* **1998**, *32*, 3743−3748.

Received for review September 9, 2005. Revised manuscript received November 2, 2005. Accepted December 5, 2005.

ES051794Q